Chirality-induced asymmetric magnetic nucleation in Pt/Co/AlOx ultrathin microstructures

Stefania Pizzini, Jan Vogel, Stanislas Rohart, Liliana-Daniela Buda, E. Jué, Olivier Boulle, Ioan Mihai Miron, C.K. Safeer, Stéphane Auffret, Gilles Gaudin, et al.

Chirality-induced asymmetric magnetic nucleation in Pt/Co/AlOx ultrathin microstructures

S. Pizzini,[1,2,*] J. Vogel,[1,2] S. Rohart,[3] L.D. Buda-Prejbeanu,[4] E. Jué,[4]
O. Boulle,[4] I.M. Miron,[4] C.K. Safeer,[4] S. Auffret,[4] G. Gaudin,[4] and A. Thiaville[3]

[1] *CNRS, Institut Néel, 38042 Grenoble, France*
[2] *Univ. Grenoble Alpes, Institut Néel, 38042 Grenoble, France*
[3] *Laboratoire de Physique des Solides, Univ. Paris-Sud, CNRS UMR 8502, 91405 Orsay, France*
[4] *SPINTEC, UMR 8191, CEA/CNRS/UJF/Grenoble-INP, INAC, 38054 Grenoble Cedex, France*

(Dated: March 18, 2014)

The nucleation of reversed magnetic domains in $Pt/Co/AlO_x$ microstructures with perpendicular anisotropy was studied experimentally in the presence of an in-plane magnetic field. For large enough in-plane field, nucleation was observed preferentially at an edge of the sample normal to this field. The position at which nucleation takes place was observed to depend in a chiral way on the initial magnetization and applied field directions. An explanation of these results is proposed, based on the existence of a sizable Dzyaloshinskii-Moriya interaction in this sample. Another consequence of this interaction is that the energy of domain walls can become negative for in-plane fields smaller than the effective anisotropy field.

PACS numbers: 75.70.Ak, 75.60.Jk

Current-induced domain wall motion in magnetic nanostrips with perpendicular magnetic anisotropy (PMA) is the subject of intense studies. Driving a train of very narrow ($\simeq 10$ nm) domain walls (DW) in the same direction and at high velocity has important potential applications in all-magnetic memories [1] or logic circuits. The large DW velocities and their motion against the electron flow found for non-centrosymmetric stacks, in which a magnetic layer is in contact with a heavy metal on one side only, cannot be explained in terms of the spin-transfer torque (STT) [2] alone. Several torques deriving from spin-orbit interactions at the interfaces or in the bulk of the heavy metallic layers have to be taken into account. Two main mechanisms giving rise to spin-orbit torques (SOT) have been identified, the Rashba effect [3–5] and the Spin Hall effect (SHE) [4, 6, 7].

Recently, it was shown that the large velocities of current-driven domain walls and their direction of motion in $Pt/Co/AlO_x$ could be understood if domain walls were assumed to have Néel internal structure and a fixed chirality [8]. Such domain walls, called Dzyaloshinskii domain walls (DDW), are stabilized by the presence of a non-compensated interfacial Dzyaloshinskii-Moriya interaction (DMI) [9, 10]. This interaction, which derives from the combination of low structural symmetry and strong spin-orbit coupling, favours helicoidal magnetic structures and skyrmion lattices if the interaction is strong [11–14] or DW with a fixed structure and chirality for a weaker interaction [8, 13, 15]. The anti-damping SOT associated to the absorption, at the Pt/Co interface, of the spin current generated by SHE in the Pt layer can then explain the large velocities of DDW.

The presence or not of DMI in ultrathin films with PMA is still under debate, calling for additional experiments. Very high resolution magnetic microscopy is the privileged technique to directly investigate the internal structure of such narrow domain walls. Recent experiments using spin-polarized LEEM have indeed shown that, in $Pt/(Co/Ni)_n$ multilayers, domain walls are of the Néel type [15]. The presence of chiral Néel DW may be also highlighted by less demanding experiments in which field and current-driven DW dynamics are studied in the presence of an in-plane magnetic field, applied normal to the DW. In several non-centrosymmetric stacks, $\downarrow\uparrow$ domain walls (separating up and down domains) and $\uparrow\downarrow$ DW have been found to move at different speeds, depending on the strength and the direction of the in-plane field. The symmetry of this effect has been considered as a proof that DW have Néel internal structure and a fixed chirality [16–19]. Field-driven measurements [19] can address more directly the effect of an in-plane field on the internal DW structure and therefore on DW dynamics, because of the absence of the effective fields induced by STT and SOT in the case of current-driven dynamics.

In this Letter we show for $Pt/Co/AlO_x$ microstructures a new kind of chiral effect: in the presence of an in-plane magnetic field, nucleation of reversed domains takes place preferentially at one edge of the sample, oriented perpendicular to this field. The side at which nucleation takes place depends on the direction of both in-plane field and initial magnetization. The asymmetry is thus chiral, and we show that DMI can explain this.

The experiments were carried out on Pt(3 nm)/Co(0.6 nm)/AlO_x(2 nm) layers patterned by electron beam lithography into two large injection pads connected by micrometric strips. The strips were used for field and current-driven domain wall dynamics (not shown here) while the nucleation experiments were carried out on the pads. The films were deposited on a Si/SiO_2 substrate by magnetron sputtering. Samples

were oxidized *in situ* by oxygen plasma in order to induce PMA. Magnetization reversal was studied using magneto-optical Kerr microscopy. In each experiment, magnetization is first saturated with an out-of-plane magnetic field (H_z). Nucleation of reversed domains is then induced by an opposite H_z field pulse, under a DC in-plane field H_x. Several samples with similar composition and varying magnetic anisotropy have been measured.

Figure 1 illustrates an example of the occurrence of chiral nucleation and the symmetry of this effect. When an H_z field pulse (amplitude $18-20$ mT and length $50-100$ ms) is applied antiparallel to the initial magnetization direction, magnetization reversal is initiated by the nucleation of a reversed domain at a particular spot of the sample, away from the edges, corresponding a local defect (Fig. 1(a)). When a sufficiently strong in-plane field H_x is applied at the same time as H_z, new nucleation centers appear at one edge of the pad. Starting from positive ($\uparrow$) saturation (corresponding to dark contrast in the Kerr images), a positive H_x field (along the positive x axis) promotes nucleation of reversed $\downarrow$ domains at the left side of the sample (Fig. 1(c-e)). As the amplitude of H_x increases, the nucleation probability increases but no nucleation appears at the right edge of the sample, up to $\mu_0 H_x = 260$ mT. If either the initial magnetization direction or the H_x field direction is reversed, the nucleation takes place at the opposite side. Figures 1(e-f) show indeed that nucleation takes place at the right side when a negative H_x field is applied starting from the same $\uparrow$ saturation. Similarly, nucleation takes place on the right side when H_x is kept positive but the initial magnetization is reversed ($\downarrow$) (Fig. 1(g-h)). This shows that the observed asymmetry is in fact chiral.

The nucleation field $H_{z,n}$ was measured as a function of H_x for a sample having an anisotropy field of 700 mT (slightly weaker than that of the sample shown in Fig. 1) both for a defect within the film and at the sample edges. The length of the H_z pulse was fixed at 20 ms. For a defect within the film, $H_{z,n}$ was defined as the field for which the domain appears with 100% probability. For the edges, $H_{z,n}$ was defined as the field for which 10-15 domains systematically nucleate [20]. The main result of these measurements, shown in Fig. 2, is that while the nucleation field of a domain within the film is almost H_x-field independent, $H_{z,n}$ strongly decreases with the in-plane field for the domains nucleating at the sample edges.

The chiral behavior of magnetization reversal cannot be explained by simply invoking a local reduction of anisotropy along the sample edges, which would keep the symmetry between opposite edges. In order to explain the observed chiral nucleation, a phenomenon which breaks the symmetry of the system when an H_x field is applied has to be invoked. A possible origin of this phenomenon is the presence in non-centrosymmetric

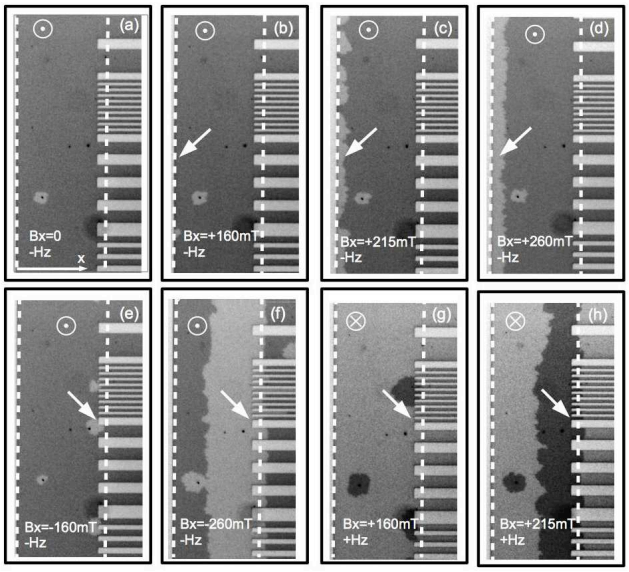

FIG. 1. Kerr images showing the chiral nucleation of domains at one side of the pad of the Pt/Co/AlO_x microstructure, by application of an out-of-plane field pulse. (a)-(d): magnetization is initially saturated $\uparrow$ and B_x=0, +160, +215 and +260 mT; (e-f) magnetization is initially saturated $\uparrow$ and B_x =-160 mT and -260 mT; (g)-(h) magnetization is initially saturated $\downarrow$ and B_x is +160 mT and +260 mT. The width of the pad is 70 μm. The dotted lines highlight the left and right edges of the pad and the arrows show the side of the sample where nucleation takes place.

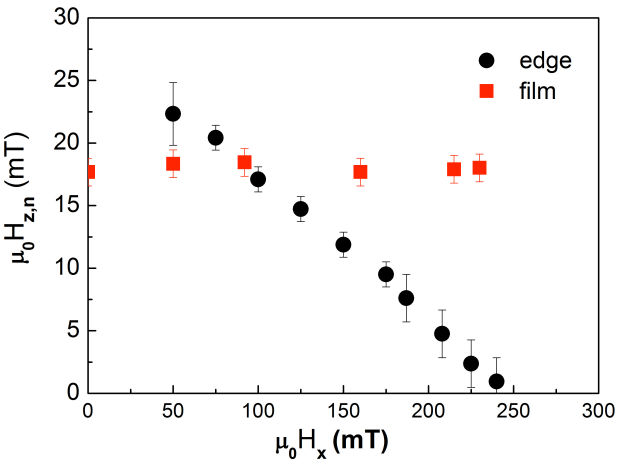

FIG. 2. (color online). Nucleation fields measured as a function of in-plane field H_x for the reversed domain in the middle (squares) and at the left edge of the sample (circles). Note the difference of scales between the two axes.

Pt/Co/AlO_x stacks of a non-vanishing DM interaction which stabilizes Néel walls. We thus quantitatively investigate this hypothesis using two models.

Zero temperature model. In real samples (i.e. including defects), magnetization reversal is controlled by few defects acting as nucleation centers [21]. Chiral nucleation

requires defects with a chiral micromagnetic structure around them. DMI provides such a state at sample edges, inducing locally a tilt of the magnetization [22]. When an in-plane field normal to an edge is applied, the tilt angle depends on its orientation (parallel or anti-parallel to the field) and favored nucleation at one edge can be expected. Using the same 1D model in the x direction normal to the edge as in [22], the edge tilt angle θ is given by

$$m_x = \sin\theta = \pm\Delta\frac{D}{2A} + \frac{H_x}{H_{K0}}, \qquad (1)$$

where D is the DMI constant, A the exchange constant, $H_{K0} = 2K_0/(\mu_0 M_s)$ the anisotropy field (K_0 is the effective anisotropy constant), $\Delta = \sqrt{A/K_0}$ the nominal domain wall width and the $\pm$ sign refers to the two edges of the sample along x. Figure 3(a) sketches the effect of H_x and H_z on the micromagnetic configurations.

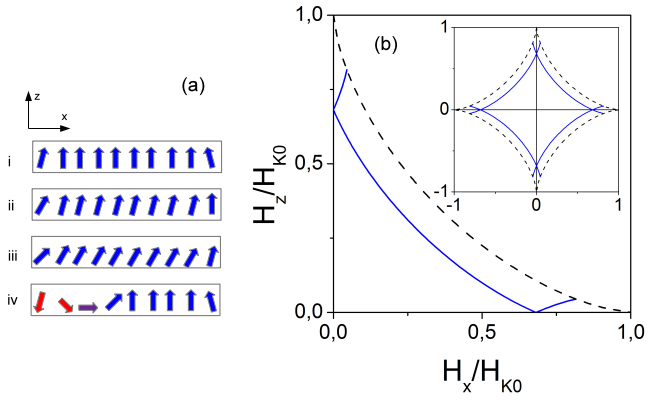

FIG. 3. (color online). a) Sketch of the micromagnetic configuration within a microstructure with DMI in zero applied field (i), under an x field (ii), under an additional negative z field (iii), and after reversal, with a domain wall of magnetization parallel to the x field (iv). b) results of a 1D calculation showing the reversal field for $D/D_{c0} = 0$ (dashes) and 0.5 (lines). For $D \neq 0$ an easy and a hard branch develop, corresponding to the reversal at the two edges of the microstructure. Inset: complete astroids.

In the absence of thermal fluctuations, the solution for the onset of magnetization instability at the edge can be mapped [20] to a solution of the Stoner-Wohlfarth model [23]. Figure 3(b) shows the reversal field H_z versus H_x (normalized to H_{K0}), calculated for different D/D_{c0} (with $D_{c0} = 4\sqrt{AK_0}/\pi \equiv \sigma_{00}/\pi$ giving the onset of the spontaneous formation of magnetization cycloids). For $D = 0$, the standard Stoner-Wohlfarth astroid is obtained and no difference occurs between the sample edge and the center. For a finite D, the edge reversal field with $H_x = 0$ decreases by a factor $[1 - (2/\pi)D/D_{c0}]$. As H_x is applied, the astroid splits into two branches revealing the difference between the two sample sides: on the side where m_x is initially parallel (resp. anti-parallel) to H_x the tilt is larger (resp. smaller) and the reversal field decreases (resp. increases) with H_x.

This model is in qualitative agreement with the experimental results: *i)* it explains why in the presence of DMI magnetic nucleation is observed only at one sample edge, *ii)* it explains qualitatively the decrease of nucleation field as the x field amplitude is increased. However, the calculated values of the nucleation field are about one order of magnitude larger than the experimental ones.

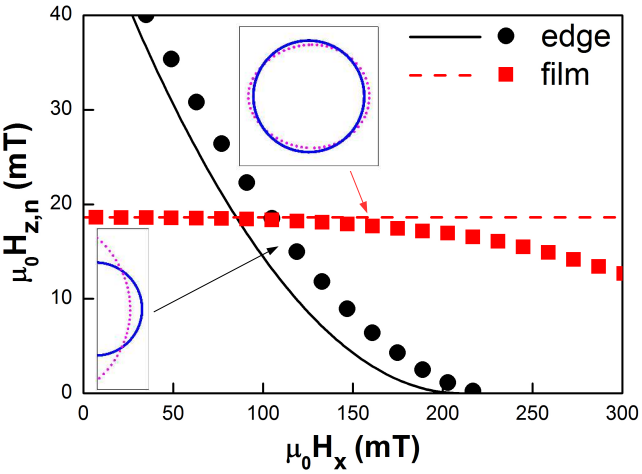

FIG. 4. (color online). Nucleation field *vs* H_x for a domain at the edge and in the film calculated using the rigid droplet model (full and dotted line) and the relaxed model (dots and square symbols). Insets: calculated droplet shapes for $H_x/H_{K0} = 0$ (lines) and 0.21 (dots).

Finite temperature model. In a macroscopic sample, magnetization reversal occurs *via* the creation of reversed domains followed by the propagation of domain walls. This is described by the so-called "droplet model" [24, 25] well-known for first order phase transitions. Let us first consider the creation of a cylindrical domain of radius R inside the film. The free energy of this droplet is:

$$E/t = 2\pi R\sigma_0 - 2\mu_0 M_s H_z \pi R^2, \qquad (2)$$

where t is the film thickness, $\sigma_0 = \sigma_{00}(1 - D/D_{c0})$ the domain wall energy density in the presence of DMI [8], and H_z the applied magnetic field. The critical droplet radius is $R_c = \sigma_0/(2\mu_0 M_s H_z)$. Below R_c the droplet collapses, whereas above R_c the domain increases its size by DW propagation. This gives rise to an energy barrier for the nucleation of the droplet:

$$E_B = \frac{\pi {\sigma_0}^2 t}{2\mu_0 M_s H_z}. \qquad (3)$$

In an Arrhenius model with attempt time τ_0, the nucleation field for a waiting time $\tau = \tau_0 e^p$ reads then:

$$H_{n,film} = \frac{\pi {\sigma_0}^2 t}{2\mu_0 M_s p k_B T} \qquad (4)$$

Under the assumption that the magnetic droplet structure is completely rigid (*i.e* no magnetization rotation in the domains nor in the domain wall, no droplet shape optimization), the application of an in-plane field H_x does not modify the energy of the droplet: the Zeeman energy gained within the half-droplet having a DW magnetization component parallel to H_x is compensated by the loss of energy within the half-droplet with opposite magnetization. This agrees with the results of Fig. 2 which show that the nucleation field for the reversed domain away from the edges does not vary with H_x.

On the other hand, the energy of a half-droplet nucleating at one edge of the sample is modified by the in-plane field. By again assuming a rigid droplet structure, its energy reads:

$$E/t = \pi R(\sigma_0 \mp 2\Delta\mu_0 M_s H_x) - \mu_0 M_s H_z \pi R^2 \quad (5)$$

where the Zeeman energy associated to the in-plane field H_x within the DW volume has been included in the DW energy. The $\mp$ sign refers to the gain/loss of Zeeman energy for a domain wall having its magnetization parallel/anti-parallel to the applied in-plane field, respectively, i.e. to the two sample edges. In analogy with the nucleation within the film, the nucleation field at the edges is then:

$$H_{n,edge} = \frac{\pi(\sigma_0 \mp 2\Delta\mu_0 M_s H_x)^2 t}{4\mu_0 M_s p k_B T} \quad (6)$$

This shows that the presence of DMI gives rise to different nucleation fields for DW having magnetization parallel or anti-parallel to H_x. In a sample with DMI, the DDW created at the two edges starting from saturation have opposite magnetization: this explains the nucleation of reversed domains only at one side of the sample and the symmetry of the effect when in-plane field direction and magnetization saturation are reversed. Note that experimentally, nucleation at the hard side of the sample is never observed at larger H_z fields, as the magnetization is always reversed by propagation of the domain walls formed at the easy side for smaller nucleation fields.

Figure 4 (lines) shows the variation of the nucleation field as a function of H_x, calculated for a droplet within the film and a half-droplet having its magnetization parallel to the applied field. The used magnetic parameters for Pt/Co/AlO_x are $A = 16$ pJ/m, M_s=1.1 MA/m, $\mu_0 H_{K0} = 700$ mT, and $D = 2.2$ mJ/m^2 ($D/D_{c0} = 0.7$).

It can be seen that the droplet model including the presence of large DMI provides an excellent understanding of the measurements: not only the different variation of $H_{z,n}$ vs. H_x within the film and at the easy edge is accounted for, but also the order of magnitude of the reversal fields at the edge is in quantitative agreement with the experiments. In the film, in order to account for the local reduction of the anisotropy field at the defect and therefore reproduce the experimental values of the nucleation field, the energy of the domain wall was reduced by a factor $\epsilon \approx 0.4$ as done previously [26].

Lifting the first two restrictions of the rigid model can be performed semi-analytically, using the 'small circle' model (the wall magnetization distribution is assumed to belong to a plane, that cuts the order parameter sphere along a small circle). This provides accurate DW energies, as was shown long ago [27] and checked again here. Once the orientation-dependent DW energy is known, the optimal droplet shape is obtained using the Wulff construction [28]. In the case of the half droplet, in full analogy with the calculation of the contact angle of a liquid droplet on a surface, the difference of edge energies for up and down domain magnetization (that can be analytically calculated with the same model as used in the Zero temperature section) was introduced in the Wulff construction. For each value of H_x, the droplet shapes were first computed (see insets in Fig. 4). Inside the film, an asymmetric elongation along the in-plane field is seen. At the edge, a significant elongation perpendicular to the field takes place, as the DW oriented perpendicular to the field has a much reduced energy and can expand its length. With the shape fixed, the determination of the critical droplet size was then performed [20]. The numerical results of this semi-analytical model, shown in Fig. 4 (symbols) for the case $D/D_{c0} = 0.7$, are very close to experiments. The new feature is the decrease of the nucleation field at the defect in the film, as the in-plane field increases. Comparing calculations and experimental data showed that, within this model, $D \geq 0.7 D_{c0}$ is required to get similar evolutions with in-plane field magnitude [20].

The decrease to zero of the nucleation field, seen both experimentally and in the model, is due to the decrease to zero of the DDW energy under a sufficiently large in-plane field. In the case of an in-plane field normal to the DDW, the DW profile can be analytically calculated for an arbitrary value of the in-plane field. For DMI-induced DW moment in the same direction as the field, the DW energy reads (with $h = H_x/H_{K0}$ [29]):

$$\sigma = \sigma_{00}[\sqrt{1-h^2} - (h + \frac{2}{\pi}\frac{D}{D_{c0}})\arccos h]. \quad (7)$$

This falls to zero at $h \approx 1 - D/D_{c0}$. For other in-plane angles between field and DW normal, the zero crossing takes place at larger fields, reaching H_{K0} when the field is along the DW. This appears to be a unique feature of the Dzyaloshinskii DW.

In conclusion, the nucleation of reversed domains in Pt/Co/AlO_x microstructures was observed to be chiral, and could be explained by the presence of a strong DM interaction within this non-centrosymmetric structure. The in-plane field favours nucleation, at one edge, of DDW having their m_x component parallel to the field. Note that edge nucleation of reversed domains bypasses the topological problem of nucleating skyrmions inside a

sample [30, 31]. Asymmetric nucleation measurements constitute a straightforward way to determine the sign of D and therefore the chirality of Néel walls. A droplet model including DMI gives quantitative agreement with the measurements, even when assuming a complete rigidity of the magnetic structures. A full treatment of the domain wall profile shows that for large DMI and in-plane field the DDW energy becomes negative, a feature hitherto unnoticed. Although all consequences of this specific feature of the Dzyaloshinskii domain walls need to be explored, we already observed nucleation of reversed domains under the application of the sole H_x field.

This work was supported by the Agence Nationale de la Recherche, project ANR 11 BS10 008 ESPERADO. SR and AT thank Jacques Miltat for discussions. SP acknowledges the support of the Nanofab team at the Institut Néel.

* stefania.pizzini@neel.cnrs.fr

[1] S. S. P. Parkin, M. Hayashi, and L. Thomas, Science **320**, 190 (2008).
[2] J. Slonczewski, J. Magn. Magn. Mater. **159**, L1 (1996).
[3] I. M. Miron, G. Gaudin, S. Auffret, B. Rodmacq, A. Schuhl, S. Pizzini, J. Vogel, and P. Gambardella, Nature Mater. **9**, 230 (2010).
[4] I. M. Miron, K. Garello, G. Gaudin, P.-J. Zermatten, M. V. Costache, S. Auffret, S. Bandiera, B. Rodmacq, A. Schuhl, and P. Gambardella, Nature **476**, 189 (2011).
[5] A. Manchon and S. Zhang, Phys. Rev. B **79**, 094422 (2009).
[6] L. Liu, O. J. Lee, T. J. Gudmundsen, D. C. Ralph, and R. A. Buhrman, Phys. Rev. Lett. **109**, 096602 (2012).
[7] K. Garello, I. M. Miron, C. O. Avci, F. Freimuth, Y. Mokrousov, S. Blügel, S. Auffret, O. Boulle, G. Gaudin, and P. Gambardella, Nature Nanotech. **8**, 587 (2013).
[8] A. Thiaville, S. Rohart, E. Jué, V. Cros, and A. Fert, EPL **100**, 57002 (2012).
[9] I. E. Dzyaloshinskii, Sov. Phys. JETP **5**, 1259 (1957).
[10] T. Moriya, Phys. Rev. **120**, 91 (1960).
[11] M. Bode, M. Heide, K. von Bergmann, P. Ferriani, S. Heinze, G. Bihlmayer, A. Kubetzka, O. Pietzsch, S. Blügel, and R. Wiesendanger, Nature **447**, 190 (2007).
[12] P. Ferriani, K. von Bergmann, E. Y. Vedmedenko, S. Heinze, M. Bode, M. Heide, G. Bihlmayer, S. Blügel, and R. Wiesendanger, Phys. Rev. Lett. **101**, 027201 (2008).
[13] S. Meckler, N. Mikuszeit, A. Pressler, E. Y. Vedmedenko, O. Pietzsch, and R. Wiesendanger, Phys. Rev. Lett. **103**, 157201 (2009).
[14] S. Heinze, K. von Bergmann, M. Menzel, J. Brede, A. Kubetzka, R. Wiesendanger, G. Bihlmayer, and S. Blügel, Nature Phys. **7**, 713 (2011).
[15] G. Chen, T. Ma, A. T. N'Diaye, H. Kwon, C. Won, Y. Wu, and A. K. Schmid, Nature Commun. **4**, 2671 (2013).
[16] K.-S. Ryu, L. Thomas, S.-H. Yang, and S. Parkin, Nature Nanotech. **8**, 527 (2013).
[17] S. Emori, U. Bauer, S.-M. Ahn, E. Martinez, and G. S. D. Beach, Nature Mater. **12**, 611 (2013).
[18] P. P. J. Haazen, E. Murè, J. H. Franken, R. Lavrijsen, H. J. M. Swagten, and B. Koopmans, Nature Mater. **12**, 299 (2013).
[19] S.-G. Je, D.-H. Kim, S.-C. Yoo, B.-C. Min, K.-J. Lee, and S.-B. Choe, Phys. Rev. B **88**, 214401 (2013).
[20] Supplemental material available at http://link.aps.org gives more information about the experimental technique and procedure, details the solution of the zero temperature model, shows full numerical micromagnetic simulation results, explains how the micromagnetic parameters of the sample were estimated, and discusses the absolute size of the critical droplets.
[21] A. Aharoni, Rev. Mod. Phys. **34**, 227 (1962).
[22] S. Rohart and A. Thiaville, Phys. Rev. B **88**, 184422 (2013).
[23] E. C. Stoner and E. P. Wohlfarth, Phil. Trans. Roy. Soc. London **A240**, 599 (1948), reprinted in IEEE Trans. Magn., vol. 27, pp. 3475-3518 (1991).
[24] B. Barbara and M. Uehara, IEEE Trans. Magn. **83**, 997 (1976).
[25] B. Barbara, J. Magn. Magn. Mater. **129**, 79 (1994).
[26] J. Moritz, B. Dieny, J. P. Nozières, Y. Pennec, J. Camarero, and S. Pizzini, Phys. Rev. B **71**, 100402 (2005).
[27] A. Hubert, *Theorie der Domänenwände in geordneten Medien(in german)* (Springer Verlag, 1974).
[28] M. C. Desjonquères and D. Spanjaard, *Concepts in Surface Physics*, Springer Series in Surface Sciences, vol. 30 (Springer, Berlin, 1996).
[29] The calculation without DMI can be found in [27].
[30] J. Sampaio, V. Cros, S. Rohart, A. Thiaville, and A. Fert, Nature Nanotechn. **8**, 839 (2013).
[31] O. J. Lee, L. Q. Liu, C. F. Pai, Y. Li, H. W. Tseng, P. G. Gowtham, J. P. Park, D. C. Ralph, and R. A. Buhrman, Phys. Rev. B **89**, 024418 (2014).